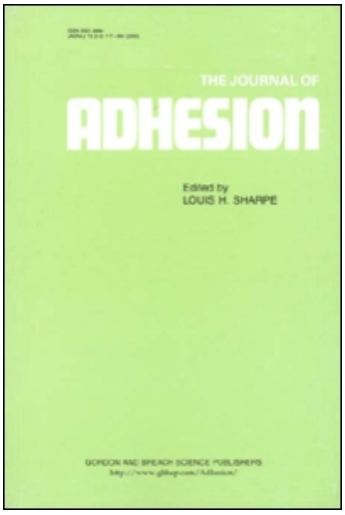

The Journal of Adhesion

Publication details, including instructions for authors and subscription information:
http://www.informaworld.com/smpp/title~content=t713453635

Adhesion on Microstructured Surfaces

Emilie Verneuil[a]; Benoît Ladoux[b]; Axel Buguin[a]; Pascal Silberzan[a]
[a] Laboratoire Physico Chimie Curie (UMR 168), Institut Curie, Centre de Recherche, Paris, France [b] Laboratoire MSC (UMR 7057), Université Paris, Paris, France

To cite this Article Verneuil, Emilie , Ladoux, Benoît , Buguin, Axel and Silberzan, Pascal(2007) 'Adhesion on Microstructured Surfaces', The Journal of Adhesion, 83: 5, 449 — 472
To link to this Article: DOI: 10.1080/00218460701377529
URL: http://dx.doi.org/10.1080/00218460701377529

The Journal of Adhesion, 83:449–472, 2007

ISSN: 0021-8464 print/1545-5823 online
DOI: 10.1080/00218460701377529

Taylor & Francis
Taylor & Francis Group

Adhesion on Microstructured Surfaces

Emilie Verneuil
Laboratoire Physico Chimie Curie (UMR 168), Institut Curie, Centre de Recherche, Paris, France

Benoît Ladoux
Laboratoire MSC (UMR 7057), Université Paris, Paris, France

Axel Buguin
Pascal Silberzan
Laboratoire Physico Chimie Curie (UMR 168), Institut Curie, Centre de Recherche, Paris, France

Using a homemade setup, we investigated the adhesion between soft elastic substrates bearing surface microstructures (array of caps [resp., holes] of height [resp., depth] h) and a smooth surface of the same rubber. In the framework of the classical model developed by Johnson, Kendall, and Roberts, we show the following. (i) The existence of a critical height h_c for the microstructures, resulting from a competition between the adhesion energy and the elastic deformation energy necessary to invade the pattern: for $h < h_c$, the bead and the substrate are in intimate contact even when the applied force is zero, and for $h > h_c$, an air film remains intercalated in the microstructure, and the contact is limited to the top of the caps or between the holes. The transition between these two states can be induced by increasing the squeezing force. (ii) The adhesion energy, W, of intimate contacts ($h < h_c$) decreases as the height increases. Suspended contacts correspond to a low adhesion and a nearly Hertzian behavior.

Using simple scaling arguments and a two-level energetic description (single microstructure and whole contact) we propose a semiquantitative description of these observations.

Keywords: Adhesion; Elastomers; Gecko; JKR; Microstructures; Roughness

Received 19 November 2006; in final form 20 March 2007.

One of a Collection of papers honoring Liliane Léger, the recipient in February 2007 of The *Adhesion Society Award for Excellence in Adhesion Science, Sponsored by 3M*.

Address correspondence to Pascal Silberzan or Axel Buguin, Physico-Chimie Curie, Institut Curie, Centre de Recherche, UMR 168, 26 Rue d'Ulm, F-75248 Paris, France. E-mail: pascal.silberzan@curie.fr or axel.buguin@curie.fr

INTRODUCTION

Contacts between elastic bodies have been widely studied as early as the end of the 19th century, starting with the theory developed by Hertz in 1882 [1] describing the elastic strains induced when two spherical elastic lenses are put in contact. However, the Hertz model does not take into account the adhesion between two bodies, which is usually not negligible for real systems. A century later, an adhesive contribution was added to this description in two different ways: a first model was developed by Johnson, Kendall, and Roberts (JKR, 1971 [2]), and another one by Derjaguin, Muller, and Toporov (DMT, 1975 [3]). These two models were unified few years later first by Muller *et al.* [4] and then by Maugis [5]. Whereas the DMT description applies quite well to hard contacts [4], the JKR model is now well accepted as the best approach to describe contacts between soft bodies [6] such as the silicone rubbers used in the present study. In the following, we denote W_0 as the adhesion energy and E as the soft material Young's modulus.

In any case, Hertz, JKR, and DMT theories apply to topographically smooth substrates that seldom exist in the real world where the roughness induces a partial contact between the bodies. What then is the real contact area between rough solids? This fundamental question is of practical importance in fields as diverse as electrical or thermal conductivity of junctions, adherence of tires on roads, and control of friction forces. Hence, many studies have aimed at relating the real contact area with the applied load between rough and smooth bodies. A first method proposed by Greenwood and Williamson [7] and experimentally validated in Ref. [8] used the Hertz model to describe contacts at the scale of individual asperities. In the case of plane substrates, these authors have shown that the real contact area increases linearly with load, which is the basis for most friction models. Adhesion was introduced by Fuller and Tabor [9] and Persson [10] using the JKR model to describe the microcontacts at each asperity, whereas the roughness was modeled with either a Gaussian [9] or a self-affine [10] distribution of heights. The ability of a soft substrate to coat an asperity results from a competition between the deformation energy *via* E and the gain in surface energy *via* W_0 [10]. It has then been shown that adhesion drastically decreases with roughness, this decrease being more rapid for small elastic lengthsW_0/E. A paradox then arises for which adhesion energy can be very weak although the real contact area is a sizeable part of the apparent area. This should give rise to high friction forces with weak adhesion. Experimental evidence for such behaviors has been given in Refs. [9], [11], and [12].

In contrast with the random roughness dealt with in the studies described previously, Johnson *et al.* have modeled periodic one- or two-dimensional wavy surfaces in the absence [13] or presence [14] of adhesion. These authors have shown that at small load and for weakly adhesive surfaces, the system can be described by a superimposition of noninteracting Hertz or JKR contacts, whereas at higher loads, the neighboring contacts became coupled, a result confirmed in Ref. [15]. In the case of adhesive bodies, this theoretical model gives rise to a sharp transition in the variation of the contact area per asperity with the applied load.

Recent developments in microfabrication techniques offer new perspectives in making well-defined topographically structured surfaces at smaller and smaller scales that can be used in adhesion experiments as model substrates of controlled roughness. This control of adhesion *via* surface topography is a welcome addition to the well-known chemical control. In this article, we present an experimental study where the adhesion is purely controlled by the physical properties of the surfaces, *i.e.*, by their topography. Using caps or holes, we have characterized the adhesion at the scale of the entire contact as well as the contacts at each asperity. The experiments are semiquantitatively interpreted on the basis of a simple theoretical model.

MATERIALS AND METHODS

Substrates Fabrication

We have fabricated two types of microtextured substrates: surfaces patterned with an hexagonal array of spherical caps (radius $r \approx 1\,\mu$m, μm, center-to-center distance $\lambda = 4\,\mu$m) and their negative replicas, *i.e.*, surfaces with the corresponding holes.

The fabrication uses a combination of hard and soft lithography. Following a conventional photolithography step, the desired pattern is replicated on a silicon wafer by deep reactive ion etching (DRIE). After complete removal of the resist, cleaning, and activation of the surface with a plasma treatment, the wafers are silanated with tridecafluorotrichlorosilane (ABCR) in vapor phase. (This treatment has been used systematically in the course of the present study to facilitate unmolding or to lower the surface energy and is generically denoted "silanization" hereafter.) We obtain, as a final result, hexagonal patterns of holes (with depths h ranging from 100 nm to 1 μm) in silanated silicon wafers [16].

A curable polydimethysiloxane PDMS (Sylgard 184, Dow Corning, Midland, MI, USA) is poured on these molds and cured at 65°C for

24 h. The cured soft elastomer (Young's modulus: $E \approx 2$ MPa) can then be easily peeled off, and we get substrates that are microstructured with spherical caps (Fig. 1a). This particular shape is a consequence of the small depths etched during the DRIE step. These surfaces can be used directly for adhesion tests or after silanization as molds to

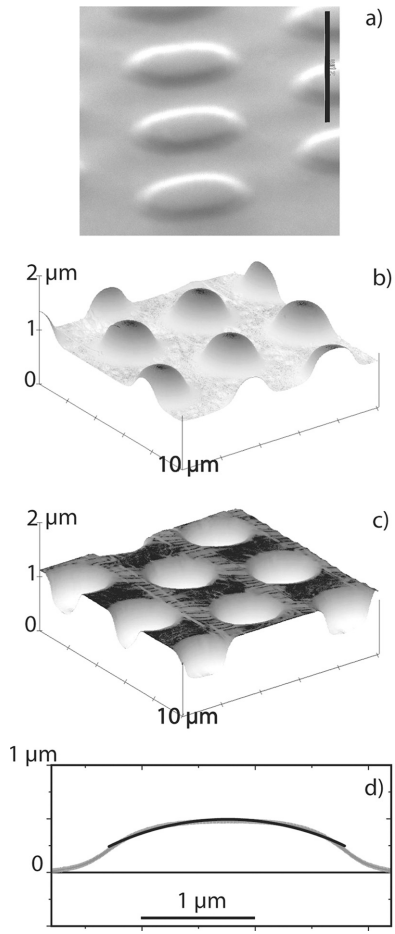

FIGURE 1 Images of substrates patterned with 470-nm-high microstructures: (a) Scanning electron micrographs of a PDMS substrate covered with caps. The bar represents 2 µm. (b) Images obtained through atomic force microscopy in contact mode of a PU substrate with holes (replica of the PDMS substrate with caps). (c) AFM topography image of a PU substrate with caps used in (d) to determine its geometrical properties.

fabricate negative replicas (*i.e.*, structured with holes) using the same process (Fig. 1b).

When a larger Young's modulus was needed so that the surface could be considered as nondeformable, we used a photocurable polyurethane (PU) (J91, Summers Optical, Hatfield, PA, USA) to replicate these substrates. Again, the silanated PDMS surfaces are used as molds for uncured PU, and cross-linking is obtained by exposure to UV light (100 W) for 15 min. After peeling off the PDMS, we get hard ($E' \approx 1.3$ GPa) PU micropatterned surfaces.

The geometrical properties (height h, radius r) of the micropatterns are characterized by atomic force microscopy (AFM) or scanning electron microscopy (SEM) (Fig. 1). These analyses also show that caps or holes can be modeled as spherical asperities (Fig. 1d) with a given radius of curvature ρ (Table 1) and that these surfaces are smooth at the nanometer scale: roughness originates only from the micropattern. In the following, the microstructures are described with a roughly constant $r \sim 1\,\mu$m and a variable h.

Flat and smooth PDMS (resp., PU) surfaces are obtained by molding on a bare silanated silicon wafer (resp., smooth silanated PDMS). They are used as reference surfaces.

Rubber beads are prepared with small droplets of uncured PDMS deposited on a silanated glass slide [17]. They adopt a spherical shape (typical contact angle $\sim 65^\circ$), and after curing, we obtain semispherical lenses with radii of curvature R ($\approx$1 mm). The radius of curvature of each bead is carefully measured at its apex by interference microscopy. Again, these lenses can be silanated to lower their surface energy.

TABLE 1 Height (or Depth) h, Radius r, and Radius of Curvature ρ of the Caps (or Holes) Obtained through AFM Measurements on the PU Replicas

PDMS caps and PU holes			PDMS holes and PU caps		
h (nm)	r (μm)	ρ (μm)	h (nm)	r (μm)	ρ (μm)
80	0.8	3.6	80	0.8	3.6
220	1.5	5.4	210	1.6	5.9
310	1.3	2.9	360	1.5	3.3
560	1.6	2.7	470	1.4	2.3
840	1.2	1.3	750	1.2	1.4

Accuracy is 10 nm for h and is 100 nm for r and ρ.

Experimental Setup

The experimental setup [18] is based on the JKR experiment principle [2]: the rubber bead is pressed against the substrate, and we measure both the squeezing force F and the contact radius a. Figure 2 gives a schematic representation of the setup.

The rubber bead is deposited at the end of a flexible glass lever (the silicone elastomer naturally adheres to the glass) whose dimensions (length 20 mm, width 1 mm, thickness 200 μm) have been chosen to yield a normal spring constant k_n well adapted to the force experienced in the present study. Based on the geometry of the lever, a rough estimation of this spring constant is $k_n \approx 20\,\mathrm{mN \cdot m^{-1}}$ [19]. Each lever is systematically individually calibrated using the added mass method [20] with an accuracy of 3%. The force applied on the rubber bead is measured through the deflection of the lever *via* the reflection of a laser at its end. The reflected beam is collected on a two-quadrant photodetector that gives access, after calibration, to the normal force F exerted by the bead on the substrate. A three-axis micromanipulator, set on the microscope stage, allows moving the bead.

The contact area is observed by interference microscopy (wavelength 546 nm). As the distance between the bead and the substrate is of the order of a few μm, interference fringes are clearly visible.

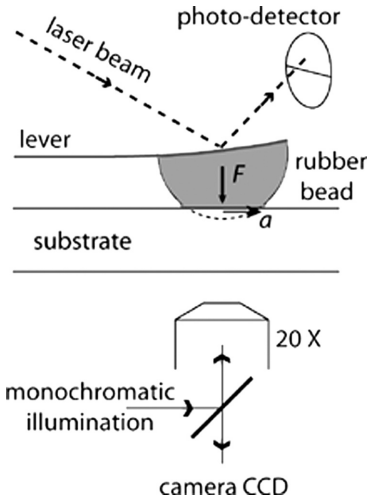

FIGURE 2 Schematic representation of the experimental setup. The contact force F between the bead and the substrate is measured through the deflection of a flexible lever using a reflected laser beam (upper part of the setup). The contact is observed by interference microscopy (lower part).

The resulting interferograms give an accurate measurement of the contact area (radius a) and, after reconstruction, of the bead profile close to the contact line [21].

Tests

We use the classical method of the so-called JKR test to measure the adhesive and elastic properties of microstructured substrates. It consists in squeezing the bead against the substrate by incremental steps (here 2.5 μm). After each compressive step, a delay of 1 minute is held to let the contact relax [22] before performing the measurement. The full compression is followed by a decompression at the same velocity. Forces applied on the contact range from -1.5 to $+1.5$ mN. Unless otherwise stated, the results reported here deal with the compression step.

RESULTS

Smooth Substrates

Smooth and flat PDMS or PU surfaces are taken as reference substrates and characterized using a soft PDMS bead through the method described in the previous section. The compression can be analyzed using the classical JKR theory [2]. This model leads to Eq. (1):

$$F = \frac{Ka^3}{R} - \sqrt{6\pi W_0 K a^3}, \tag{1}$$

where the first term is simply the Hertz contribution [1]. The second term (negative contribution) depends on the adhesion energy W_0: the force required to create a given contact area is reduced when adhesive interactions exist between surfaces. For incompressible materials, the contact stiffness K is a combination of the Young's modulus of the bead, $E_{b,}$ and the one of the substrate, E_s:

$$\frac{1}{K} = \frac{9}{16}\left(\frac{1}{E_b} + \frac{1}{E_s}\right). \tag{2}$$

In practice, we use an alternate form of Eq. (1) to determine K and W_0:

$$\frac{a^{3/2}}{R} = \frac{1}{K}\frac{F}{a^{3/2}} + \sqrt{\frac{6\pi W_0}{K}}. \tag{3}$$

The filled squares in Fig. 3 show the typical result of a JKR test performed on a smooth PDMS substrate ($a^{3/2}/R$ *versus* $F/a^{3/2}$).

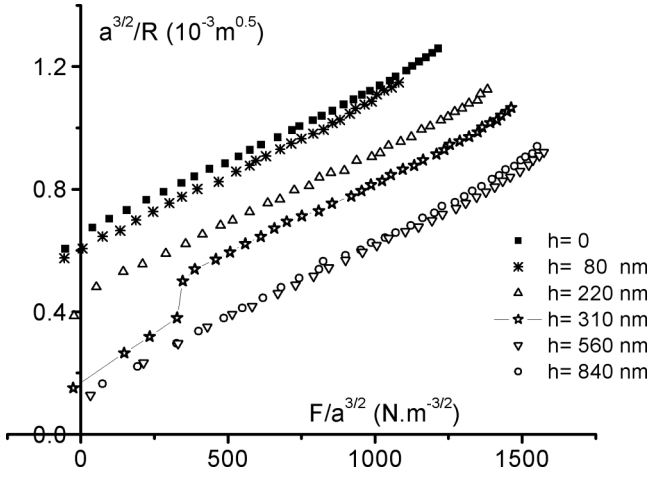

FIGURE 3 Variations of the contact force and the contact radius during the compression experiments: $F/a^{3/2}$ *versus* $a^{3/2}/R$ for a smooth PDMS substrate ($h = 0$) and the PDMS substrates with caps of various heights h. The slope of these lines is inversely proportional to the contact rigidity, and the y-axis crossing point is proportional to the square root of the adhesion energy.

A linear fit [Eq. (3)] gives the rigidity $K = 1.9 \pm 0.2\,\mathrm{MPa}$ and the adhesion energy $W_0 = 43 \pm 5\,\mathrm{mJ \cdot m^2}$ of the contact, in good agreement with previous measurements taken from the literature [17].

It is possible to define another adhesion energy W', during the decompression, by fitting the linear part of this decompression curve with Eq. (3). The adhesive hysteresis is then defined as the difference $\Delta W = W' - W_0$. Smooth PDMS surfaces lead to weak hysteresis compared with the involved adhesion energies: $\Delta W < 2\,\mathrm{mJ \cdot m^2}$. Again, this value is in good agreement with previous measurements performed on the same system [23,24] and is attributed to free oligomers in the bulk PDMS.

Using interference microscopy, one can reconstruct the contact profile near the triple line (Fig. 4, dashed line). These profiles show that the joint between the two PDMS surfaces is at right angles, which is characteristic of JKR adhesive contacts where adhesion induces normal tensile stress at the contact edge.

Surfaces and beads can be silanated to tune the adhesion energy. JKR tests then give W_0 for various combinations: $W_0^{sil} = 34 \pm 5\,\mathrm{mJ \cdot m^{-2}}$ if only one surface is silanated, and $W_0^{sil/sil} = 13 \pm 3\,\mathrm{mJ \cdot m^{-2}}$ if the treatment is applied to both surfaces. As expected [17], W_0 decreases with silanization.

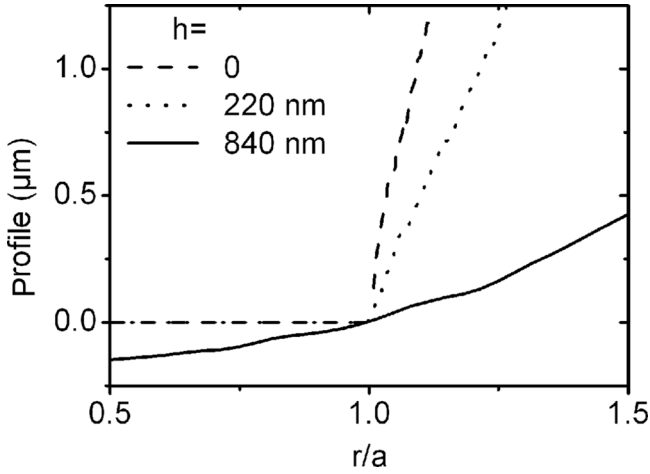

FIGURE 4 Profiles of the bead near the contact edge as a function of the normalized radial coordinate r/a for a smooth substrate ($h = 0$), an intimate contact on a microstructured substrate ($h = 220\,\text{nm}$), and a suspended contact ($h = 840\,\text{nm}$). The contact force F is zero. Smooth substrate and intimate contact join the bead at right angles, as predicted by the JKR theory, while the join is tangential for a suspended contact.

Finally, contacts of higher rigidity, *i.e.*, hard PU surfaces against a PDMS bead, have been tested. We measure $K^{hard} = 3.0 \pm 0.2\,\text{MPa}$, and an adhesion energy $W_0^{hard} = 39 \pm 5\,\text{mJ} \cdot \text{m}^{-2}$ with a bare PDMS bead and $W_0^{hard,\,sil} = 28 \pm 4\,\text{mJ} \cdot \text{m}^{-2}$ with a silanated bead. Hysteresis is weak ($4 \pm 2\,\text{mJ} \cdot \text{m}^{-2}$) with bare PDMS bead and cannot be defined in the silanated case.

Contacts between smooth substrates are used as a reference state to study the role of a microstructuration on the adhesion properties.

Soft Microstructured Substrates

For PDMS substrates patterned with spherical caps, we observe three distinct behaviors as a function of cap heights as shown in the compression sequences of Fig. 5. For the smallest heights ($h = 80\,\text{nm}$ and $220\,\text{nm}$), the contact area is dark and the pattern disappears. Because the bead and the substrate are made of the same polymer (same refractive index), this dark contact area can be attributed to an intimate contact between the bead and the substrate. For the intermediate height ($h = 310\,\text{nm}$), at small forces, the pattern is still observed under the contact, meaning that an air film remains

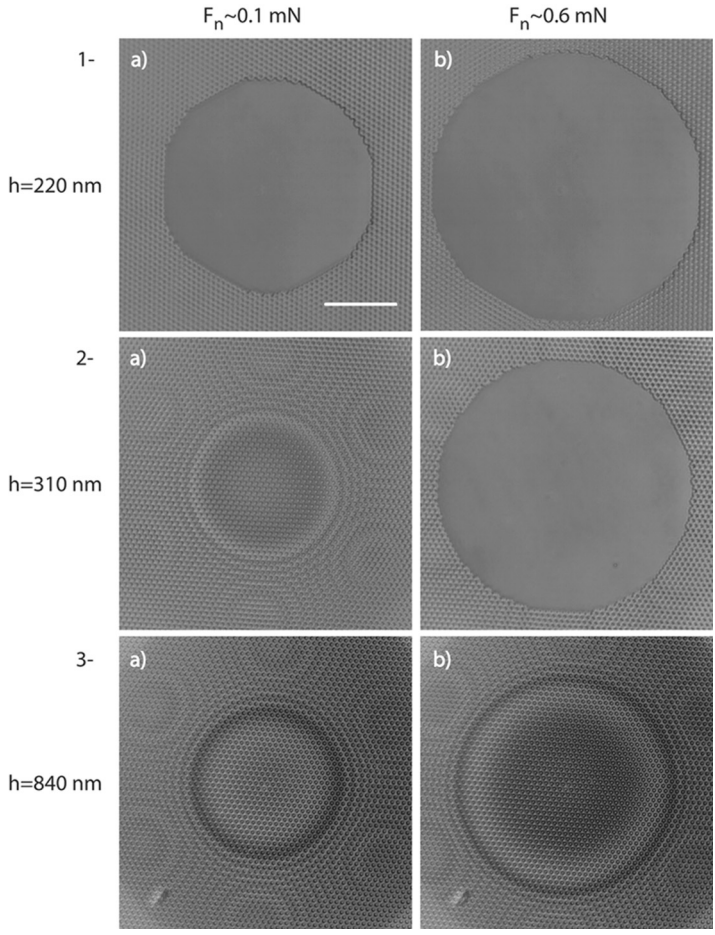

FIGURE 5 Interference microscopy images of the contact on substrates covered with caps of various heights and for two values of the contact force. The contact can be intimate (1a, 1b, and 2b) or suspended (2a, 3a, and 3b). The white bar represents 50 μm.

intercalated between the caps. This case will be called hereafter "suspended contact." However, as the applied force increases, the pattern disappears under the contact starting from a nucleation point at the contact center, similar to the dewetting of the air film. For this height, at low forces, only the tips of the asperities truly contact the bead. As the force increases past the threshold force, the contact invades the surface between the caps. For larger heights ($h = 560$ or 840 nm),

the pattern remains visible under the contact (suspended contact) in the whole range of forces that can be explored with our setup.

At this stage we define a critical height h_c for the caps so that a transition between suspended and intimate contacts is observed at zero contact force. The previous experimental observations give a framing of h_c: $220\,\text{nm} < h_c < 310\,\text{nm}$.

Force and contact radius measurements during a compression are shown in Fig. 3 for micropatterned surfaces (open symbols). From these curves, assuming the JKR description still holds, we determine values for K and W. We find that the contact rigidity K is the same as for smooth substrates whatever the height of the structures: $K^{\text{PDMS}} = 1.9 \pm 0.2\,\text{MPa}$. On the other hand, the adhesion energy, W, is strongly affected by the pattern. The variation of W/W_0 with h is plotted in Fig. 6. In the case of intimate contacts (filled squares), W decreases with h, whereas suspended contacts (open triangles) yield a low adhesion energy compared with the adhesion of smooth surfaces ($W/W_0^{\text{PDMS}} \approx 4\%$). This last value does not depend on h within our experimental accuracy.

We have also measured the adhesive hysteresis from the decompression curves. In the case of intimate contacts, the hysteresis is enhanced and increases with h from $1\,\text{mJ}\cdot\text{m}^{-2}$ to $14\,\text{mJ}\cdot\text{m}^{-2}$, whereas

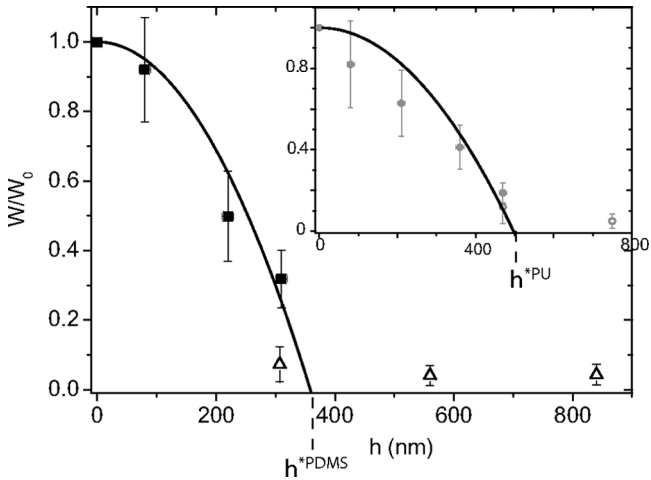

FIGURE 6 Adhesion energy W normalized by W_0 as a function of the caps height h (PDMS/PDMS contacts). Inset: Values for PU hard substrates covered with caps. For intimate contacts (full symbols), W/W_0 decreases with h and is well described with Eq. (12) (lines). Above h^*, suspended contacts are observed (open symbols).

it remains small and close to the smooth substrate value for suspended contacts ($\Delta W = 4 \pm 4\,\mathrm{mJ \cdot m^{-2}}$). The transition from suspended to intimate contacts induced by the normal load (for $h = 310\,\mathrm{nm}$) is only visible for the compression. During the decompression, the intercalated air layer between caps is never restored until the contact ruptures.

Through interference microscopy, we can determine the bead profile for various loads. These profiles are shown in Fig. 4 for an intimate contact (dotted line) and a suspended contact (solid line), in comparison with the smooth substrate (dashed line). Similar to smooth substrates, intimate contacts correspond to a JKR profile with a vertical tangent at the contact edge. This observation is another signature of the presence of adhesion between the two surfaces. In contrast, the bead and the substrate remain tangent in the case of suspended contacts, which is typical of low adhesion systems. In this case, the profile is also visible *inside* the contact area thanks to the intercalated air layer. The caps are more squeezed at the center than at the edge, which can simply be attributed to the normal stress field distribution [2,25] that reaches a maximum at the center of the contact.

Influence of the Adhesion Energy

With silanated beads and substrates, we can compare these results for different adhesion energies. After such modifications, the main features (the existence of the intimate and suspended contacts) are qualitatively still observed. However, quantitatively, the critical height h_c varies with the adhesion energy. We get $80\,\mathrm{nm} < h_c^{sil} < 310\,\mathrm{nm}$ and $h_c^{sil/sil} < 80\,\mathrm{nm}$ for one or both silanated surfaces, respectively. Thus, h_c decreases as the adhesion becomes weaker.

Influence of the Contact Stiffness

Rigid PU substrates patterned with caps yield the same regimes with increasing cap heights: first, for small values of h, intimate contacts at all forces; second, for intermediate values, there is a critical force separating regimes of intimate and suspended contacts; and finally, for larger values of h, suspended contacts at all forces (in the range of forces explored with the present setup). The critical height h_c is here measured to be between 360 nm and 470 nm. As for PDMS substrates, the adhesion energy, W/W_0^{PU}, decreases with h (Fig. 6 inset) for intimate contacts and drops to weak values ($W/W_0^{\mathrm{PU}} = 5\%$) for suspended contacts ($h > 470\,\mathrm{nm}$). Finally, the rigidity, K^{PU}, is roughly constant for both flat and patterned substrates ($K^{\mathrm{PU}} = 3.5 \pm 0.2\,\mathrm{MPa}$) in good agreement with Eq. (2).

Caps versus Holes

The same JKR test was used with the complementary replicas, *i.e.*, substrates patterned with holes. Some similarities with the substrates with caps can be noticed: For holes shallower than a threshold depth h_c, the whole contact is of the intimate type similar to caps (Fig. 7a). Interestingly, this critical depth has the same value as the critical height measured on substrates with caps ($h_c \sim 310\,\text{nm}$ for untreated surfaces). Compared with smooth surfaces, the intimate contacts ($h < h_c$) correspond to an enhanced adhesive hysteresis ($\Delta W \sim 10\,\text{mJ}/\text{m}^2$) that increases as the holes' depth increases, showing again a strong similarity with the caps.

A major difference between caps and holes appears when holes are deeper than h_c. Although the transition from a suspended state to an intimate one can still be triggered by increasing the contact force (without any transition in the JKR curve), the intimate state nucleated at the contact center does not propagate to the whole contact and remains limited to its central region (radius a_c). Thus, for the transiting substrates, coexistence between the suspended and intimate contacts can be observed (Fig. 7b) for compression and decompression. In this case, during the decompression, the edge of the contact retracts on the suspended region while the size of the central region stays nearly constant until the edge of the contact reaches the collapsed area. It corresponds to a smooth transition on the JKR curve (results not shown). Consequently, the hysteresis is not defined, but the pull-off force is drastically enhanced, as it increases by 30% in comparison with smooth substrates. For even deeper holes, the contacts are suspended whatever the accessible external load (Fig. 7c).

Compared with smooth substrates, the adhesion energy is smaller for contacts involving a surface patterned with holes ($W \sim 30\,\text{mJ} \cdot \text{m}^{-2}$), as was observed for caps. However, surprisingly, there is no dependence of this energy on the depth of the holes. The adhesion energy is nearly constant and is not affected by the state of the contact (intimate, mixed, or suspended) or the appearance of the intimate contact zone of the transiting substrates (Fig. 8).

INTERPRETATION AND DISCUSSION

As the substrates and beads used here are typically a couple of millimeters thick compared with contact radii smaller than 100 μm, the conditions of semi-infinite media are met for the JKR theory [26].

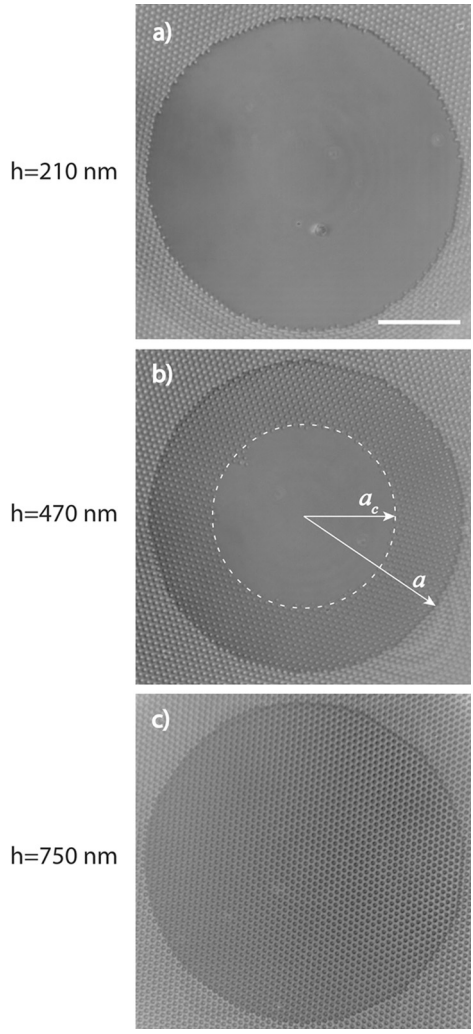

FIGURE 7 Interference microscopy images of the contacts on substrates with holes of various depths and for a positive load $F = 0.6\,\text{mN}$. The contact is intimate for $h < h_c$ (a), mixed with an intimate zone at the center of a suspended contact for $h_c < h < h^*$ (b), and suspended for $h > h^*$ (c). The white bar represents $50\,\mu\text{m}$.

Intimate versus Suspended Contacts

Equation (1), valid at the scale of the whole contact, can also be used to describe a contact at the level of a single cap [8,9] (at this scale the

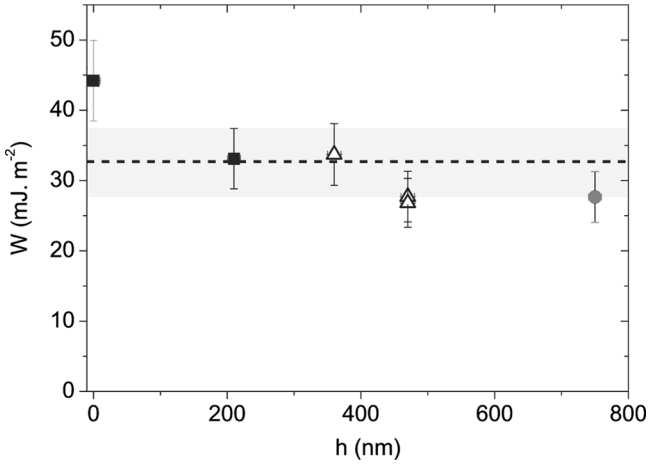

FIGURE 8 Adhesion energy W as a function of the holes' depth h for PDMS substrates structured with holes. At low depths, the contacts are always intimate contacts (filled squares). Above the critical depth, h_c, a transition between a suspended and a mixed suspended/intimate contact can be induced through an increase of the force (open triangles). For deeper holes, the contact remains suspended in our range of forces (gray circles). The dotted line is a fit of the data with Eq. (15).

rubber bead can be seen as a flat surface). We denote a_1 the contact radius for this asperity, F_1 the corresponding local contact force (σ_1 being the corresponding normal stress), ρ the cap's radius of curvature, and W_0 the adhesion energy between the smooth PDMS surfaces. Without external load on the whole contact, there is still a force distribution under the contact; however, as the suspended contact case corresponds to a weak adhesion energy, W, the local force, F_1, can be neglected in front of the adhesive term ρW_0 and at this scale Eq. (1) leads to

$$a_1^3 = h_0 \rho^2 \tag{4}$$

where $h_0 = 6\pi(W_0/K)$ is the so-called elastic length.

In the absence of external load and starting from a suspended situation, a criterion for collapse is that the size of the contact becomes of the order of the radius, r, at the basis of the cap radius itself: $a_1 \approx r$. Assuming that the cap is a portion of a sphere ($\rho \approx r^2/2h$ for $h \ll r$), we obtain the critical height h_c:

$$h_c \approx \frac{1}{2}\sqrt{rh_0}. \tag{5}$$

Values for h_0 and h_c can be estimated for the PDMS/PDMS system: for $r = 1\,\mu\text{m}$: $h_0 = 410\,\text{nm}$ and $h_c \sim 400\,\text{nm}$. If we keep in mind the rough assumptions leading to this result, it agrees reasonably well with the experimental observation that $h_c \approx 200 - 300\,\text{nm}$. Because r is fixed, Eq. (5) also predicts that $h_c \propto \sqrt{h_0} \propto \sqrt{W_0}$. This conclusion is in qualitative agreement with the experimental results on silanated substrates because we find that h_c indeed decreases for less adhesive surfaces.

Regarding the role of contact rigidity, however, a direct comparison with the experiments performed on hard PU substrates shows a slight increase of h_c for a contact stiffness about two times as large [*cf.* Eq. (2)], although Eq. (5) predicts $h_c \propto 1/\sqrt{K}$, meaning, from Eq. 2, that the new h_c should be divided by $\sqrt{2}$. The origin of this discrepancy may be attributed to minor corrections mainly due to a variation of the PDMS cap radius under compression (Poisson's ratio $\sim\frac{1}{2}$) and the assumption that the cap keeps its spherical shape even at large deformations for soft substrates. These two points should introduce different numerical factors between hard and soft surfaces. Moreover, the assumption of total independence between adjacent pillars can also be questioned at that point. From a qualitative point of view, one expects from Eq. (5) suspended contacts on the whole range of thicknesses ($h_c \to 0$), even for a large elastic modulus.

Equation (5) can be derived differently using an energy balance and simple scaling arguments. With no external force, the free energy, $\Im_s$, of a single cap in the suspended regime results from two contributions: the elastic deformation and the gain in surface energy. The transition from a suspended to an intimate contact is obtained when the contact radius $a_1 \approx r$. Thus, ignoring numerical factors, $\Im_s$ can be estimated at the transition

$$\Im_s \approx K\left(\frac{h}{r}\right)^2 r^3 - W_0 r^2 \approx Kr(h^2 - h_c^2) \tag{6}$$

where we have identified $h_c \approx \sqrt{rh_0}$.

Because the change of sign of the free energy is equivalent to an energy minimization in a scaling description, we can conclude that for $h > h_c$ the free energy is positive and no transition occurs, whereas for $h < h_c$, $\Im_s$ is negative and the intimate contact is preferred. This analysis applies to zero external force and only allows determining the equilibrium state just after the contact has been established during a compression experiment.

It is instructive to estimate the normal external force $F = F_c$ required to observe the transition between suspended and intimate contacts. Keeping a scaling approach, the work ($\sim F_1 \cdot h$) needed to

squeeze a single microstructure is then added to Eq. (6), leading to

$$\Im_s \approx K\left(\frac{h}{r}\right)^2 r^3 - W_0 r^2 - \sigma_1 r^2 h \approx h r^2(\sigma_c - \sigma_1) \tag{7}$$

where

$$\sigma_c = W_0 \frac{1}{h h_c^2}(h^2 - h_c^2) \tag{8}$$

As the experimentally accessible parameter is the normal force, F, let us write the equation linking F and σ_1. The transition always occurs at the contact center, as a direct consequence of the axisymmetric stress field distribution with a maximum at the contact center. The Hertz theory gives

$$\sigma_1 = \frac{3}{2\pi\phi}\left(\frac{K^2 F}{R^2}\right)^{1/3}. \tag{9}$$

The surface fraction covered by the caps, ϕ, accounts for the effective surface reduction due to the pattern (the stress only applies on the caps). Finally, the critical force is

$$F_c \approx KR^2\phi^3 \cdot \left[\frac{h_0}{h h_c^2}(h^2 - h_c^2)\right]^3 \approx \frac{KR^2\phi^3}{r^3}(h - h_c)^3. \tag{10}$$

The last equality of Eq. (10) is written in the limit of $h \sim h_c$.

Equation (10) shows that cap heights lower than h_c correspond to negative critical forces: for these heights an intimate contact is observed whatever the applied force, a result consistent with our previous conclusions. Let us note that a more rigorous calculation based on the expression of the JKR force [Eq. (1)] on one cap yields the same result [27].

Because the range of forces accessible with our experimental setup is limited, we have been able to measure a critical force for only one height for each system: for $h = 310\,\text{nm}$ in the PDMS/PDMS case and h = 80 nm if both surfaces are silanated. In fact, for caps higher than h_c, F_c increases rapidly with h ($\alpha\ h^3$), which explains why the transition is observed only in one case. Given the accuracy of our measurements, it makes more sense to compare the value of h_c inferred from Eq. (10) at the point where a force-induced transition has been observed, with the framing given by the experiments. The theoretical values, $h_c \sim 200\,\text{nm}$ for untreated PDMS surfaces and $h_c \sim 50\,\text{nm}$ if both surfaces are silanated, are again in good agreement with the experimental framing: $220\,\text{nm} < h_c < 310\,\text{nm}$ in the untreated

case and $h_c \sim 100\,\text{nm}$ for silanated surfaces, thus confirming the relevance of the model.

After the nucleation of an intimate contact at the center, its spontaneous propagation to the whole contact area is ensured by the adhesion energy due to an increase in the real contact area (the bead adhering to the substrate between caps). The corresponding gain in surface energy locally increases the stress, which becomes large enough to overcome the critical stress under the whole contact. The suspended state can be seen as a metastable state for the system.

Let us note at this point that, dealing with a hexagonal array of caps, the space between the caps is interconnected, allowing the propagation of the collapsed state. Our simple description predicts a very different behavior if this propagation is stopped along one direction: for example, for an array of lines. A further study of these effects on more subtle geometries such as mazes or percolated/unpercolated two-dimensional surfaces would be very interesting in many respects.

Adhesion Energy for the Whole Contact

To estimate the adhesion energy at the contact scale, let us come back to an energetic description. Here, we have to separate the two regimes:

For "suspended contacts" ($h > h_c$), at zero contact force, the adhesive contribution to the free energy is $W_0 a_1^2 n$ where $n \approx \phi(a/r)^2$ is the number of caps involved in the contact area and a_1 is the contact radius for each cap [Eq. (4)]. Thus, the adhesion energy for suspended contacts is given by

$$W \approx \phi W_0 \frac{(h_0 \rho^2)^{2/3}}{r^2}. \tag{11}$$

With PDMS substrates ($h_0 = 410\,\text{nm}$, $\rho = 2\,\mu\text{m}$, and $\phi = 6\%$) we find $W/W_0 \approx 8\%$, close to the experimental value ($\approx 4\%$). The exact variations of W with h_0 or ρ, however, could not be measured, as the ranges of accessible ρ (1.5 to $5\,\mu\text{m}$) and h_0 (410 to 130 nm) are too narrow.

For "intimate contacts" ($h < h_c$), the adhesion energy, W, results from a competition between the gain in surface energy for the caps approximated by $W_0 r^2/\phi$ and the elastic contribution needed to coat a cap $K.h^2 r$ ($= (W_0/h_0) \cdot h^2 r$). The contribution due to the surface increase can be neglected in front of the elastic term for caps radii larger than h_0. Because the number of caps involved in the contact is

unchanged ($\approx \phi a^2/r^2$), this equality leads to

$$W = W_0\left(1 - \left(\frac{h}{h^*}\right)^2\right) \tag{12}$$

where we have introduced the new threshold height h^*:

$$h^* = \sqrt{\frac{rh_0}{\phi}}. \tag{13}$$

Figure 6 shows the best fit (lines) with Eq. (12) for the experimental measurements with h^* as the only adjustable parameter. The model accounts well for the measured variations of *W(h)*. For PDMS substrates, the fit gives $h^* = 360\,\text{nm}$, whereas Eq. (13) gives a value of 600 nm. The scaling approach used in our description accounts well for the orders of magnitude of the experimental results.

In both analyses (intimate and suspended contacts), the elastic contribution to the free energy due to the elastic deformation of the bead and the substrate (when it is made of PDMS) leads to a contact rigidity, K, which is the same as for smooth substrates. This result is not surprising because the Young's modulus is associated with the bulk elastic strains that extend to a volume of the order of a^3 (far larger than the volume of the thin cap layer $\approx a^2h$) in both elastic media. This conclusion agrees with the experimental data, as indeed we find a contact rigidity nearly independent of h.

Interestingly, we measure an increase of hysteresis with h for intimate contacts. In the case of bare PDMS or PU substrates, because the hysteresis was negligible on smooth surfaces, it is here clearly correlated to the geometrical patterning of the surface. A quantitative analysis of the hysteresis is more difficult because it would require a precise description of the crack propagation during the decompression experiment. Because such a description is out of the scope of the present study, we stay at the qualitative level. However, this high hysteresis may be of great importance for many practical applications.

Caps versus Holes

Following the same approach, we can estimate the critical values for the holes' depth and the contact force for which a transition from a suspended to an intimate contact is observed. Let us note that because of the topology of the pattern, the intrinsic permeability of silicone elastomers to air is a key point that governs the kinetics of formation of this collapsed area. There would be no collapse for materials not permeable to the surrounding fluid (liquid or gas). Given the permeation

coefficient of the PDMS to nitrogen ($245 \cdot 10^{-10}$ cm^3.cm/cm^2.s.cmHg) [28], there is ample time for the air contained in a hole to escape through the material during an elementary compression step (or to fill it during decompression).

Omitting again all numerical factors, the free energy of an intimate contact on holes is also given by Eq. (7), leading to the critical depth $h_c(holes) \approx \sqrt{r \cdot h_0}$. The critical force that can induce the collapse is still given by Eq. 8 with $\sigma_1^c = F_1^c/(\pi \cdot r^2)$. The experiments confirm these conclusions because intimate contacts were observed for zero contact force, F, at a depth equal to the critical height of caps. The variations of the critical depth with h_0 are also in good agreement with our prediction, because decreasing h_0 by silanization leads to a decrease in the experimental values for the critical depth.

However, the propagation of an intimate contact, nucleated above a critical stress, differs notably between caps and holes. For holes, the intimate contact propagation needs a further increase in the contact force, F, whereas it is spontaneous in the case of caps. A direct consequence of this situation is the coexistence in the same contact of an intimate contact in the center and a suspended one at the periphery.

The critical stress beyond which the contact collapses in the holes can be estimated using the JKR stress distribution [2]. The measurements of both the radius of the intimate contact part, a_c, and the radius of the whole contact, a, allow one to evaluate the stress at the radial position, a_c, that limits the suspended holes from the collapsed ones. By hypothesis, this stress is equal to σ_c, and we get

$$\sigma_c = \frac{3aK}{2\pi R}\sqrt{1-\frac{a_c^2}{a^2}} + \sqrt{\frac{3WK}{2\pi a}}\frac{1}{\sqrt{1-a_c^2/a^2}}, \tag{14}$$

The estimation of σ_c through Eq. (14) as a function of a for $h = 470$ nm shows that the edge of the intimate contact part corresponds to a stress value that is approximately constant *versus* a during the whole compression phase. The order of magnitude obtained in this way for σ_c ($5.3\ 10^4$ Pa) is in agreement with the value obtained from Eq. (8) ($6.4\ 10^4$ Pa).

Finally, we can derive the adhesion energy for suspended contacts; the main term is the adhesion energy of the surfaces in contact out of the holes. The work of the applied load and the elastic and adhesive energies due to the penetration of the bead in the holes are negligible. Thus

$$W(h) = W_0(1-\phi). \tag{15}$$

This expression also applies to the intimate case and the adhesion energy on substrates with holes is independent of h and of the contact's nature.

The numerical value from Eq. (15) is plotted as the dotted line in Fig. 8; the gray area is the accuracy on W_0 and, thus, on, W ($\sim$13%). There is a good agreement between theory and experiments.

CONCLUSION

Although the influence of roughness on adhesion properties between two surfaces has many practical implications, experiments dealing with real rough surfaces are usually difficult to interpret because of the distribution of involved characteristic lengths.

The model microfabricated elastomeric surfaces used in the present study circumvent this difficulty in a way similar to how a well-defined pattern can affect the wetting properties of a substrate [29]. Along this line, there is quite a strong analogy with the so-called Cassie–Baxter to Wenzel wetting transition [30].

To summarize, we have investigated the adhesion of such substrates, and we show the following:

- There exists a critical height for the microstructure above which an air film remains intercalated under the contact area (suspended contact).
- For caps, this suspended state is metastable because above a given squeezing force the two surfaces come in to intimate contact at a nucleation point. This contact then propagates to the whole contact area.
- For holes, the same behavior is observed except that the intimate contact does not propagate and stays limited to the central region of the contact area.

The observed phenomena and in particular the evolution of the adhesion energy with the height of the structures can then be quantitatively interpreted with simple scaling arguments.

Our study also leads to some problems that would be quite fascinating to study. We list here a few of them.

We have tested here very symmetric geometries (hexagonal array of caps or holes). The main difference between these two situations is in the propagation of the intimate state to the whole contact because the transition from suspended to intimate contacts needs first a nucleation point and then a continuous path to propagate from one pattern to the next. An anisotropic pattern either *via* the distribution of elementary patterns or through their shape (the more drastic case being an array of lines) should result in an anisotropy for the whole contact. It would

be interesting to investigate more deeply this prediction and to correlate it with the example of animals that develop fibrillar and/or lamellar structures [31] at the tip of their legs to adhere on various substrates.

The permeability of silicone elastomers to gases and the quasistatic way the experiments are performed are also points deserving further investigation. For our system, the air entrapped in the holes has enough time to escape through the PDMS. However, it is possible to play on this parameter, for instance, by using less permeable rubbers or by performing the experiments in a liquid medium such as water. One then expects interesting kinetic effects such as suction-cup effects. As a matter of fact, conducting the experiments at different timescales should lead to the same result, providing that during a slow compression the entrapped medium has enough time to escape, whereas this is not the case for a fast decompression. This situation should lead to a strong hysteresis.

Finally, let us mention that we have restricted ourselves here to purely elastic substrates. The use of dissipative materials in conjunction with surface textures is a potentially powerful way to modulate the adhesion [32]. A natural extension of the present work would be its application to friction phenomena. Preliminary experiments have shown that friction can induce the coexistence between the suspended and intimate contacts under the same contact (Fig. 9). More experiments are under way in these two directions.

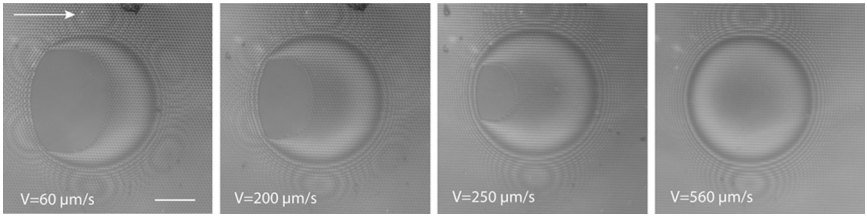

FIGURE 9 Interference microscopy images of contacts on a substrate with caps ($h = 560\,\text{nm}$) translated at various velocities, V, while the normal load is maintained at 0.7 mN. In the static regime, the contact is suspended. The arrow indicates the direction of translation of the substrate (bottom view). Starting from a situation where an intimate contact has been nucleated by a defect, a dynamically stabilized suspended/intimate contact can be observed at finite velocity, V. The size of the intimate part of the contact decreases with V. The bar represents 50 µm.

ACKNOWLEDGMENTS

It is a pleasure to thank F. Brochard, J. Clain, P. Fabre, C. Frétigny, and C. Gay for their helpful comments on our results, H. Montès for elastomer characterizations, and R. H. Austin for facilitating our access to microfabrication facilities. We acknowledge financial support from the Agence Nationale de la Recherche (programme PNANO).

REFERENCES

[1] Hertz, H., *Miscellaneous Papers* (Macmillan, London, 1896).
[2] Johnson, K. L., Kendall, K., and Roberts, A. D., *Proc. Roy. Soc. London A* **324**, 301–313 (1971).
[3] Derjaguin, B. V., Muller V. M., Toporov, Y. P., *J. Colloid. Interf. Sci.* **53**, 314–326 (1975).
[4] Muller, V. M., Yushenko V. S., and Derlaguin, B. V., *J. Colloid. Interf. Sci.* **77**, 91–101 (1980).
[5] Maugis, D., *J. Colloid. Interf. Sci.* **150**, 243–296 (1992).
[6] Johnson, K. L., *Contact Mechanics* (Cambridge Univ. Press, Cambridge, 1985).
[7] Grenwood, J. A. and Williamson, J. B. P., *Proc. Roy. Soc. London A* **295**, 300–319 (1966).
[8] Williamson, J. B. P., *Proc. Inst. Mech. Eng.* **182**, 21–30 (1967).
[9] Fuller, K. N. G. and Tabor, D., *Proc. Roy. Soc. London A* **345**, 327–342 (1975).
[10] Persson, B. N. J., *Phys. Rev. Lett.* **89**, 245502 (2002).
[11] Briggs, G. A. D. and Briscoe, B. J., *J. Phys. D* **10**, 2453–2466 (1977).
[12] Fuller, K. N. G. and Roberts, A. D., *J. Phys. D* **14**, 221–239 (1981).
[13] Johnson, K. L., Greenwood, J. A., and Higginson, J. G., *Int. J. Mech. Sci.* **27**, 383396 (1985).
[14] Johnson, K. L., *Int. J. Solid Structures* **32**, 423–430 (1995).
[15] Hui, C. Y., Lin, Y. Y., Barney, J. M., and Kramer, E. J., *J. Polym. Sci. B: Polym. Phys.* **39**, 1195–1214 (2001).
[16] du Roure, O., Saez, A., Buguin, A., Austin, R. H., Chavrier, P., Silberzan, P., and Ladoux, B., *Proc. Nat. Acad. Sci. USA* **102**, 2390–2395 (2005).
[17] Chaudhury, M. K. and Whitesides, G. M., *Langmuir* **7**, 1013–1025 (1991).
[18] Martin, A., Clain, J., Buguin, A., and Brochard-Wyart, F., *Phys. Rev. E* **65**, 031605 (2002); Clain, J., *Friction sèche et mouillée*, PhD Thesis, Université Paris 6, 2004.
[19] Landau, L. and Lifchitz, F., *Physique théorique, Théorie de l'élasticité* (Mir, Moscow, 1967).
[20] Cleveland, J. P., Manne, S., Bocek, D., and Hansma, P. K., *Rev. Sci. Instr.* **64**, 403–405 (1993).
[21] Roberts, A. D. and Tabor, D., *Proc. Roy. Soc. A.* **325**, 323–345 (1971).
[22] Maugis, D. and Barquins, M., *J. Phys. D: Appl. Phys.* **11**, 1989–2023 (1978).
[23] Silberzan, P., Perutz, S., Kramer E. J., and Chaudhury M. K., *Langmuir* **10**, 2566–2570 (1994).
[24] Choi, G. Y., Kim, S., and Ulman, A., *Langmuir* **13**, 6333–6338 (1997).
[25] Verneuil, E., Buguin, A., and Silberzan, P. to be published.
[26] Shull, K. R., Ahn, D., and Mowery, C. L., *Langmuir* **13**, 1799–1804 (1997).
[27] We thank one of the referees for pointing out this point to us.
[28] Singh, A., Freeman, B. D., and Pinnau, I., *J. Poly. Sci. B* **36**, 289–301 (1998).

[29] Bico, J., Marzolin, C., and Quéré, D., *Europhys. Lett.* **47**, 220–226 (1999); Bartolo, D., Bouamrirène, F., Verneuil, E., Buguin, A., Silberzan, P., and Moulinet, S., *Europhys. Lett.* **74**, 299–305 (2006).
[30] Wenzel, R. N., *Ind. Eng. Chem.* **28**, 988–994 (1936); Cassie, A. B. D., and Baxter, S., *Trans. Faraday Soc.* **40**, 546–551 (1944).
[31] Huber, G., Mantz, H., Spolenak, R, Mecke, K., Jacobs, K., Gorb, S. N., and Arzt, E. *Proc. Nat. Acad. Sci. USA* **102**, 16293–16296 (2005).
[32] Lamblet, M., Verneuil, E., Vilmin, T., Buguin, A., Silberzan, P., and Léger, L., in press.